Geomechanics and Engineering, *Vol. 21, No. 2 (2020) 187-200*
DOI: https://doi.org/10.12989/gae.2020.21.2.187

Study on the behaviour of pre-existing single piles to adjacent shield tunnelling by considering the changes in the tunnel face pressures and the locations of the pile tips

Young-Jin Jeon[a], Seung-Chan Jeon[b], Sang-Joon Jeon[b] and Cheol-Ju Lee*

Department of Civil Engineering, Kangwon National University, Chuncheon, Korea

(Received December 11, 2019, Revised January 16, 2020, Accepted March 2, 2020)

Abstract. In the current work, a series of three-dimensional finite element analyses have been conducted to investigate the behaviour of pre-existing single piles in response to adjacent tunnelling by considering the tunnel face pressures and the relative locations of the pile tips with respect to the tunnel. Via numerical modelling, the effect of the face pressures on the pile behaviour has been analysed. In addition, the analyses have concentrated on the ground settlements, the pile head settlements and the shear stress transfer mechanism at the pile-soil interface. The settlements of the pile directly above the tunnel crown (with a vertical distance between the pile tip and the tunnel crown of 0.25D, where D is the tunnel diameter) with a face pressure of 50% of the in situ horizontal soil stress at the tunnel springline decreased by approximately 38% compared to the corresponding pile settlements with the minimum face pressure, namely, 25% of the in situ horizontal soil stress at the tunnel springline. Furthermore, the smaller the face pressure is, the larger the tunnelling-induced ground movements, the axial pile forces and the interface shear stresses. The ground settlements and the pile settlements were heavily affected by the face pressures and the positions of the pile tip with respect to the tunnel. When the piles were inside the tunnel influence zone, tensile forces were induced on piles, while compressive pile forces were expected to develop for piles that are outside the influence zone and on the boundary. In addition, the computed results have been compared with relevant previous studies that were reported in the literature. The behaviour of the piles that is triggered by adjacent tunnelling has been extensively examined and analysed by considering the several key features in substantial detail.

Keywords: numerical modelling and analysis; shear transfer mechanism; shield TBM; soil-structure interaction; tunnel face pressure; tunnel influence zone

1. Introduction

Recently, various tunnelling activities have been conducted in urban areas, where ground excavation might affect the engineering behaviour of pre-existing adjacent piled foundations (Lee 2012). Tunnelling below or adjacent to existing piles can influence the serviceability and, in the worst-case scenarios, the stability of the piled foundations due to the tunnelling-induced ground movements, which result in pile deformations and changes in the pile forces (Lee 2012). Williamson (2014) has analysed most of the relevant studies that have been conducted in substantial detail. Numerous studies on this problem have been conducted based on theoretical methods and laboratory tests or geotechnical centrifuge tests (Jacobsz 2002, Lee and Ng 2005, Ong *et al*. 2006, Pang 2006, Cheng *et al.* 2007, Lee and Chiang 2007, Marshall 2009, Lee 2012, 2013, Ng *et al.* 2013, Dias and Bezuijen 2014a, b, Hartono *et al.* 2014, Liu *et al.* 2014, Ng and Lu 2014, Ng *et al.* 2014, Williamson 2014, Lee *et al.* 2016, Lee 2016, Raid *et al.* 2016, Oh *et al.* 2018, Soomro *et al.* 2018). Compared to these works, field measurements from full-scale tests are limited. However, Selemetas (2005), Pang (2006), Liu *et al.* (2014), Mair and Williamson (2014) and Williamson (2014) have reported measured pile behaviour from field measurements. Fig. 1 shows a sectional view of a large-diameter shield TBM(tunnel boring machine) tunnel site in Shanghai, China, which was reported by Liu *et al.* (2014). The authors analysed the pile behaviour in response to tunnelling when the piles are located laterally based on field measurements and numerical analyses.

The shield TBM method, which can minimise the ground deformation in response to tunnelling, has emerged as an optimal alternative to the conventional tunnelling method (NATM). Studies on shield TBM have been actively conducted; however, the behaviour of the piles that are adjacent to shield TBM has not attracted the interest of engineers and has yet to be clarified. Kaalberg *et al.* (2005) analysed the behaviour of the piles and the ground surface settlements in response to TBM tunnelling based on numerical analysis and field measurements. They identified the influence zone of tunnel excavation by considering the relative locations of pile tips. Mroueh and Shahrour (2008) analysed the settlements of the ground surface and the surrounding soil near the tunnel according to the stress release due to tunnelling and the tunnel advancement under

*Corresponding author, Professor
E-mail: cj32@kangwon.ac.kr
[a]Post-Graduate Student, Ph.D.
[b]Post-Graduate Student, M.Eng.

Copyright © 2020 Techno-Press, Ltd.
http://www.techno-press.org/?journal=gae&subpage=7
ISSN: 2005-307X (Print), 2092-6219 (Online)

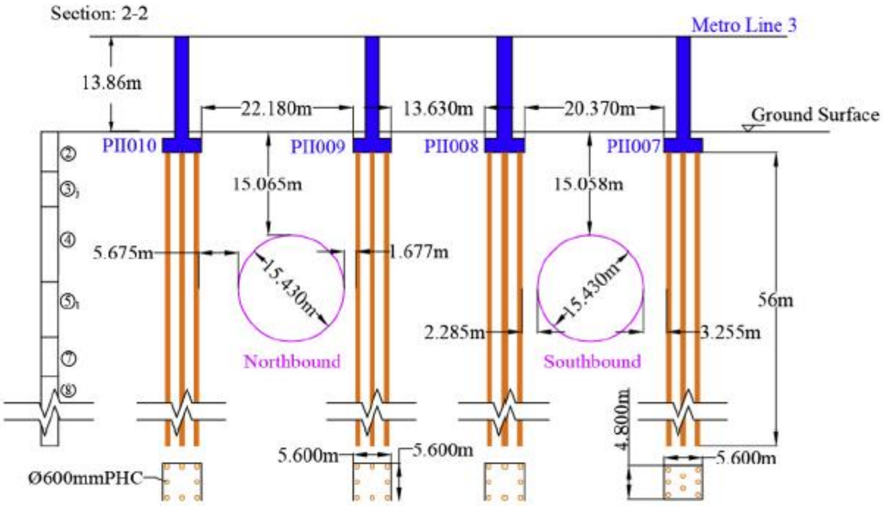

Fig. 1 Sectional view of a tunnel that crosses a bridge foundation (Liu *et al*. 2014)

constant face pressure. Lee *et al.* (2012) conducted a numerical analysis of the behaviours of structures by simulating TBM tunnelling while considering the distance of the tunnel from the upper structures. They reported that the conditions of the construction site should be considered in tunnelling because the behaviour of a structure depends heavily on the distance between the structure and the tunnel. Lee *et al.* (2012), Cho *et al.* (2014a, b), Xu *et al.* (2015), You and Kim (2017), and Ahn *et al.* (2018) have reported analyses of the ground settlements and behaviour of the piles that are caused by adjacent TBM tunnelling; however, they did not consider the face pressures.

In this study, the behaviours of the ground and piles in response to adjacent shield TBM tunnelling according to the distance of the pile tips from the tunnel were studied by considering changes of the face pressures via a series of three-dimensional (3D) finite element analyses. In addition, the effects of tunnelling on the piles were identified by analysing the tunnelling-induced pile head settlements, the axial pile forces, the relative shear displacements and the shear transfer mechanism at the pile-soil interface.

2. Numerical modelling

2.1 Finite element mesh and boundary conditions

In the current study, a three-dimensional (3D) finite element programme, namely, Plaxis 3D (2018), was used for the numerical analyses to study the behaviour of the piles by simulating the shield TBM method while considering the relative locations of the pile tips with respect to the tunnel and various face pressures. Fig. 2 presents a finite element mesh that is used in the numerical analyses. The representative geometry of the current analysis is shown in Fig. 3(a). Additionally, Fig. 3(b) shows the locations of the pile tips with respect to the tunnel and the tunnel influence zone represented by the dotted line. The tunnel diameter (D) in the analysis was 8 m with segmental thickness (t=0.25 m), and the tunnel springline

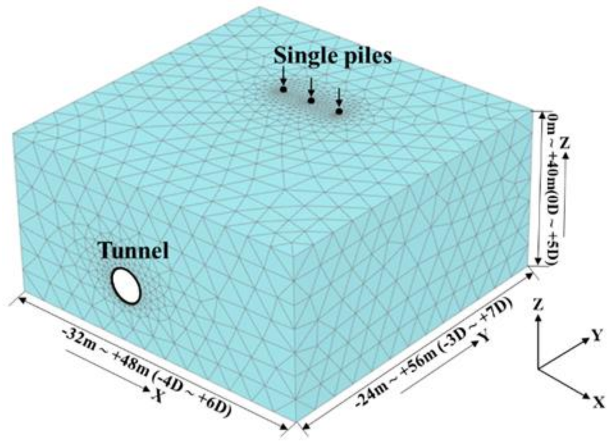

Fig. 2 Representative 3D finite element mesh that is used in the current study (the pile centre is located at Y/D=3.5, where D is the tunnel diameter)

was located at a depth of 26 m below the ground surface. The piles were assumed to be 14 m~20 m in length L_p and 0.5 m in diameter d. This corresponds to V_p = 0.25D~1.00D, where V_p is the vertical distance between the tunnel crown and the pile tip. The locations of the piles were arranged to be at offsets of H_p = 0.0D~2.0D, where D is the tunnel diameter and H_p is the distance between the tunnel centreline and the centre of the piles in the horizontal direction, as shown in Fig. 3(a). To simulate the shield TBM, a machine of 9 m in length was applied on plate elements, and the length of the segment was 1.5 m, as shown in Fig. 4. Hence, the ground was excavated 1.5 m in each increment (Plaxis 3D 2018). Additionally, it was assumed that there were 15-m-long pre-installed segments prior to tunnel advancement, as presented in Fig. 4. The details of the tunnel excavation process will be discussed in substantial detail in Section 2.3.

A constant face pressure is applied on the tunnel face to analysis the behaviour of piles qualitatively following Mroueh and Shahrour (2008) rather than assuming a linear increase in the face pressures and the value of the face pressure was calculated as $F \times Z \times \gamma \times K_o$ in consideration of

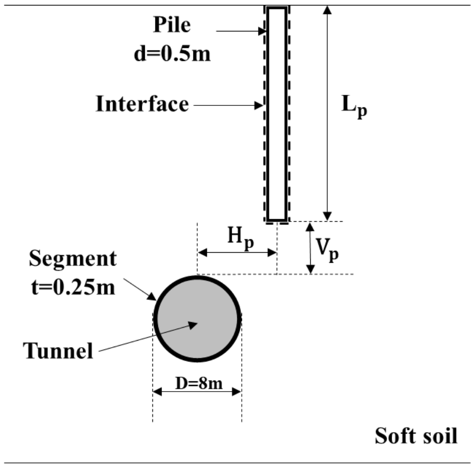

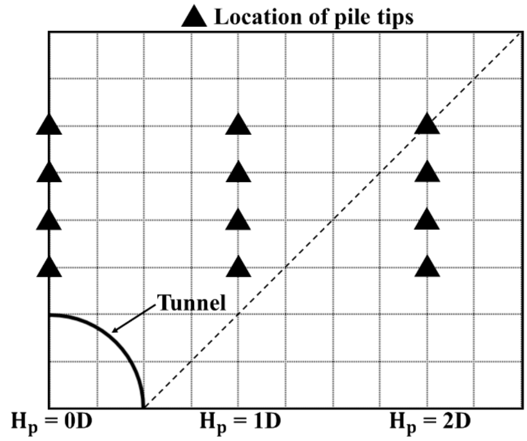

Fig. 3 (a) Sectional view of the analysis geometry and (b) Locations of the pile tips that are assumed in the current study

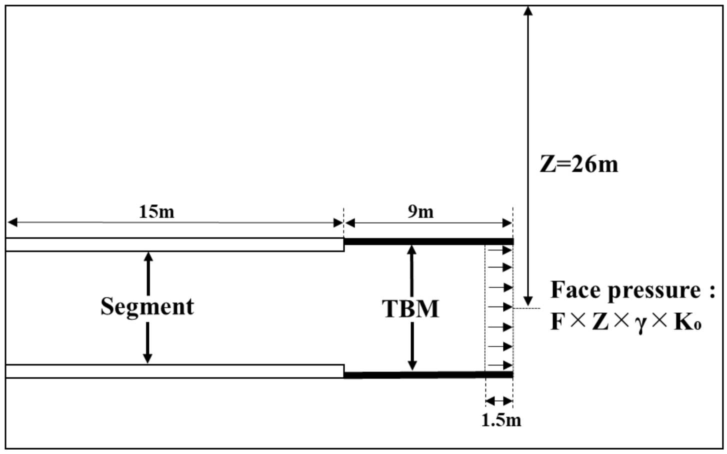

Fig. 4 Modelling of TBM tunnelling and the application of tunnel face pressure (F = the change in the tunnel face pressure (0.25-1.00), Z = the distance from the soil surface to the tunnel springline (26 m), γ = the unit weight of the material, and K_o= the lateral earth pressure coefficient at rest)

the distance from the ground surface to the tunnel springline (Mroueh and Shahrour 2008), where F is the change in the face pressure (0.25~1.00) in response to the in situ vertical soil stress prior to tunnelling, Z is the distance from the surface to the tunnel springline, γ is the unit weight of the soil, and K_o is the lateral earth pressure coefficient at rest. Table 1 summarises the numerical analyses that were conducted in the current study. A total of 22 analyses were conducted, which included the greenfield condition and various pile tip locations with various face pressures. For the piles with H_p=0D and V_p=0.25D, 4 face pressures of 65 kPa (F=0.25), 130 kPa (F=0.50), 195 kPa (F=0.75) and 260 kPa (F=1.00) were considered for various pile tip locations, as summarised in Table 1. The minimum pressure (65 kPa) that is considered in the current study is slightly smaller than the face pressure (σ_{TC} = 86.0 kPa) that is calculated via Bolton's (1991) equation, which considers the face pressure of a tunnel collapse in sandy soil. In addition, each face pressure was considered using the load factor (LF), which is expressed in equation (2). In this case, LF is roughly approximately as the inverse of the safety factor because LF = 1 corresponds to the collapse of the tunnel.

$$\sigma_{TC} = [\frac{\gamma D}{2(K_p - 2)}] \times [1 - \left(\frac{D}{2C + D}\right)^{(K_p - 2)}] \tag{1}$$

$$LF = \frac{\gamma Z + q - \sigma_T}{\gamma Z + q - \sigma_{TC}} \tag{2}$$

where γ is the unit weight of the soil, Z is the distance from the surface to the tunnel springline, q is the surface load, σ_{TC} is the magnitude of the face pressure (86.0 kPa) at the tunnel collapse, D is the tunnel diameter, K_p is the coefficient of the passive earth pressure, and C is the distance from the ground surface to the tunnel crown. The current study has modelled a dry soil condition as Mroueh and Shahrour (2008) did in their analysis

2.2 Material parameters and constitutive models

An elastoplastic analysis was conducted to simulate tunnel construction and the pile-soil interactions that are triggered by tunnelling. The pile-soil interactions at the pile-soil interface were included by using interface elements

Table 1 Summary of the numerical analyses (D: tunnel diameter)

Analysis series	Face pressure (kPa)	LF (load factor)	Pile tip location measured from tunnel		Remarks
			H_p	V_p	
L1	-	-	-	0.25D	Pile load test, L_p = 20 m
L2	-	-	-	0.50D	Pile load test, L_p = 18 m
L3	-	-	-	0.75D	Pile load test, L_p = 16 m
L4	-	-	-	1.00D	Pile load test, L_p = 14 m
G50	130	0.90	-	-	Greenfield
FP50(H_p=0D, V_p=0.25D)	130	0.90	0D	0.25D	L_p = 20 m
FP50(H_p=0D, V_p=0.50D)	130	0.90	0D	0.50D	L_p = 18 m
FP50(H_p=0D, V_p=0.75D)	130	0.90	0D	0.75D	L_p = 16 m
FP50(H_p=0D, V_p=1.00D)	130	0.90	0D	1.00D	L_p = 14 m
FP50(H_p=1D, V_p=0.25D)	130	0.90	1D	0.25D	L_p = 20 m
FP50(H_p=1D, V_p=0.50D)	130	0.90	1D	0.50D	L_p = 18 m
FP50(H_p=1D, V_p=0.75D)	130	0.90	1D	0.75D	L_p = 16 m
FP50(H_p=1D, V_p=1.00D)	130	0.90	1D	1.00D	L_p = 14 m
FP50(H_p=2D, V_p=0.25D)	130	0.90	2D	0.25D	L_p = 20 m
FP50(H_p=2D, V_p=0.50D)	130	0.90	2D	0.50D	L_p = 18 m
FP50(H_p=2D, V_p=0.75D)	130	0.90	2D	0.75D	L_p = 16 m
FP50(H_p=2D, V_p=1.00D)	130	0.90	2D	1.00D	L_p = 14 m
FP25(H_p=0D, V_p=0.25D)	65	1.05	0D	0.25D	L_p = 20 m
FP25(H_p=1D, V_p=0.25D)	65	1.05	1D	0.25D	L_p = 20 m
FP25(H_p=2D, V_p=0.25D)	65	1.05	2D	0.25D	L_p = 20 m
FP75(H_p=0D, V_p=0.25D)	195	0.75	0D	0.25D	L_p = 20 m
FP100(H_p=0D, V_p=0.25D)	260	0.60	0D	0.25D	L_p = 20 m

*Note: FP25 [tunnel face pressure=25% of the in situ horizontal soil stress at the tunnel springline(σ_{ho})], FP50 [tunnel face pressure=0.5σ_{ho}], FP75 [tunnel face pressure=0.75σ_{ho}], and FP100 [tunnel face pressure=1.0σ_{ho}]

Table 2 Material parameters in the numerical modelling

Material	Model	γ (kN/m^3)	K_o	ν	E' (MPa)	c' (kPa)	φ'(°)
Soil (Mroueh and Shahrour 2008)	Mohr-Coulomb	20	0.5	0.3	30	5	27
TBM machine (Plaxis 3D 2018)	Elastic	247	-	-	200,000	-	-
Segment (Plaxis 3D 2018)	Elastic	27	0.01	0.1	31,000	-	-
Pile	Elastic	25	0.01	0.2	30,000	-	-

*Note: γ (unit weight of the material), K_o (lateral earth pressure coefficient at rest), ν (Poisson's ratio), E' (Young's modulus), c' (cohesion), and φ' (internal friction angle of soil)

at the sides and bases of the piles, which are represented by dotted lines in Fig. 3(a), to allow for soil slip when plastic soil yielding occurs. The shield TBM machine is represented by a plate element, which is based on general three-dimensional continuum mechanics (Plaxis 3D), and interface elements were included between the tunnel (the combination of the segment and the TBM machine) and the surrounding soil, except at the tunnel face. The assumed material parameters, which are listed in Table 2, were obtained from a previous study by Mroueh and Shahrour (2008) and by using Plaxis 3D (2018). An isotropic elastic model was used for the pile and the precast tunnel segments, and a Mohr-Coulomb model that was governed by a non-associated flow rule with an isotropic elastic modulus was used for the residual soil. The interfaces are joint elements, which enable the accurate modelling of the soil-structure interaction and can be used to simulate the thin zone of intensely shearing material at the contact between a pile and the surrounding soil (Brinkgreve *et al.* 2015). In addition, the interfaces are composed of 12-node elements that consist of six pairs of nodes, which are compatible with the 6-noded triangular sides of the soil and structure elements. The reduction in the shear strength parameters at the pile-soil interface that is associated with the pile installation effect was considered using Eqs. (3) and (4).

$$c'_{int}=R_{int} \times c'_{soil} \quad (3)$$

$$\varphi'_{int}=\tan^{-1}(R_{int} \times \tan(\varphi'_{soil})) \quad (4)$$

where c'_{int} is the adhesion at the interface, R_{int} is the strength reduction factor at the interface (0.7), c'_{soil} is the cohesion of the residual soil, φ'_{int} is the interface friction angle (19.6°) and φ'_{soil} is the internal friction angle of the soil(27.0°).

2.3 Numerical modelling procedure

In the numerical analysis, the stress changes of the ground that are associated with the effect of the pile installation are not considered. Therefore, the assumed pile in the current work is similar to a cast-in-place pile. Tunnel excavation was simulated from 0D ~ +7D (0 m ~ +56 m) in the longitudinal direction (Y). It was assumed that a segment of 15 m in length and the shield TBM machine of 9 m in length were installed prior to tunnelling, as discussed. At each step, the tunnel was excavated in a 1.5-m increment; hence, 37 excavation steps were conducted. Following the initial geostatic step, axial loads of 600 kN (L_p=20 m), 500 kN (L_p=18 m), 408 kN (L_p=16 m), and 313 kN (L_p=14 m), as determined from analyses L1, L2, L3 and L4, were applied on the pile head to simulate a service load prior to the tunnel excavation. In each analysis step, the segment assembly and the tunnel excavation were conducted simultaneously. In the case of the face pressure, the distance (Z = 26 m) from the surface to the tunnel centre, the unit weight of the soil and the lateral earth pressure coefficient at rest (K_o = 0.5) are considered, as explained in Section 2.1. The applied face pressure was constant with depth at the tunnel face. Upon completion of the numerical analysis, the axial pile force on the pile P was calculated as P =$\sigma_{zz)avg}$ $\times A_p$, where $\sigma_{zz)avg}$ is the averaged vertical stress in the pile elements at a specified elevation and A_p is the cross-sectional area of the pile. Similarly, the relative shear displacements and the interface shear stresses were also averaged.

3. Computed results

3.1 Determination of the allowable pile capacity

A series of incremental axial pile loadings were applied on the pile head to simulate a pile loading test, which enables the quantification of the load-settlement relation of the piles with various lengths. Four analyses, which are labelled as L1~L4, were conducted with identical boundary conditions to those in Fig. 3(a) and the same material parameters; however, the tunnel excavation was not included. Fig. 5 presents the relationships between the axial pile loading and the pile head settlements that are computed from these analyses, which are used to determine the allowable pile capacity. In analysis L1, a nearly linear relation was obtained between the axial pile force and the

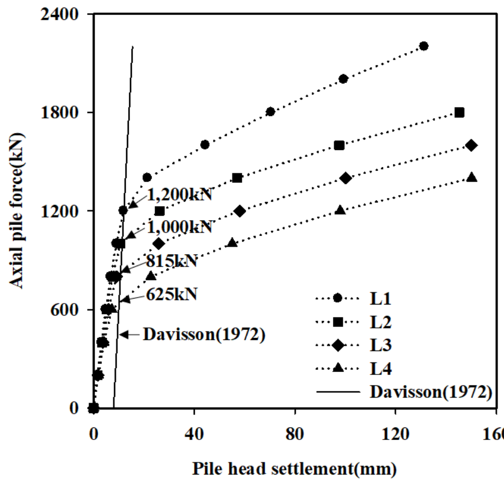

Fig. 5 Relation of the axial pile load and the pile head settlements

Table 3 Computed maximum pile head settlements and maximum axial pile forces

Analyses	Pile tip location H_p	Pile tip location V_p	Face pressure (kPa)	$\Delta_{p,net)max}/\Delta_{gr)max}$	$P_{net)max}/P_a$
FP50	0D	0.25D	130	1.62	(-)0.36
FP50	1D		130	0.67	(+)0.20
FP50	2D		130	0.23	(+)0.12
FP25	0D		65	2.59	(-)0.45
FP25	1D		65	1.26	(+)0.20
FP25	2D		65	0.57	(+)0.17
FP75	0D		195	1.17	(-)0.32
FP100	0D		260	1.10	(-)0.31

*Note: (+)ve: compression, (-)ve: tension, $\Delta_{gr)max}$: 10.8 mm, and P_a: 600 kN (L_p=20 m)

pile head settlement up to an axial pile loading of approximately 1,190 kN. However, after that threshold, a sudden increase in the pile settlement was observed with increased axial pile force, which corresponds to the development of plastic yielding of the soil that is adjacent to the pile. Similar trends have been observed in analyses L2~L4. In the current study, the widely used Davisson (1972) method was used to determine the allowable pile capacity. The Davisson (1972) empirical envelope consists of an elastic compression line and an offset, as plotted in Fig. 5. The Davisson (1972) lines for the various pile lengths (14~20 m) are almost the same; hence, only a single line is plotted in the figure for clarity. The computed load-settlement curve and the Davisson (1972) envelope coincide when the axial pile force is approximately 1,200 kN, 1,000 kN, 815 kN and 625 kN, which correspond to analyses L1, L2, L3 and L4, respectively; hence, ultimate pile capacities of 1,200 kN, 1,000 kN, 815 kN and 625 kN were deduced, as shown in Fig. 5. Then, by applying a factor of safety of 2.0, the allowable pile capacities P_a were obtained as 600 kN, 500 kN, 407.5 kN and 312.5 kN with pile head settlements Δ of 5.3 mm, 4.8 mm, 4.3 mm and 3.7 mm, which correspond to analyses L1, L2, L3 and L4,

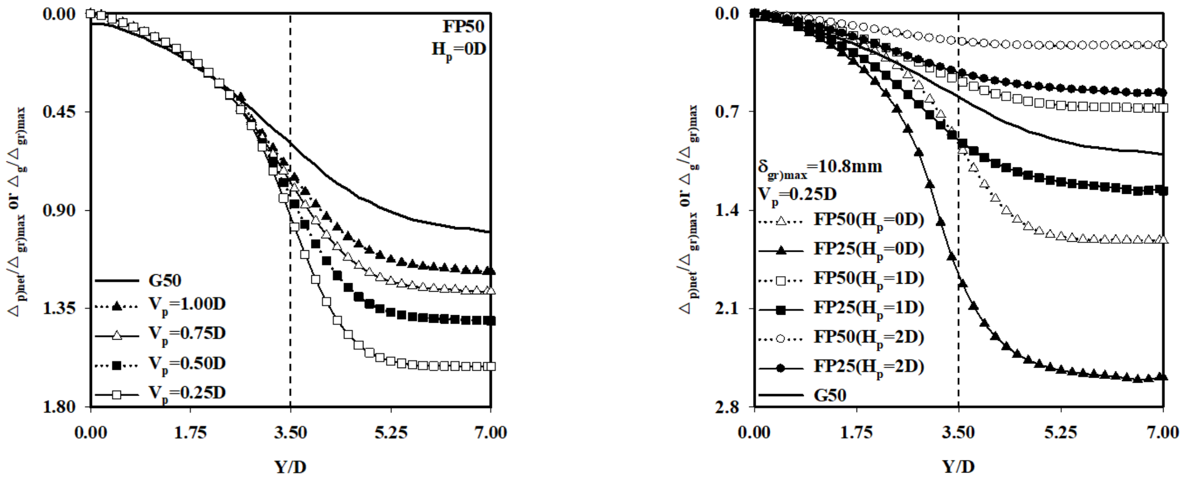

(a) (b)

Fig. 6 (a) Distributions of normalised pile head and soil surface settlements with tunnel advancement (H_p=0D and FP50) and (b) Distributions of normalised ground and pile head settlements with tunnel advancement (V_p=0.25D and L_p=20 m)

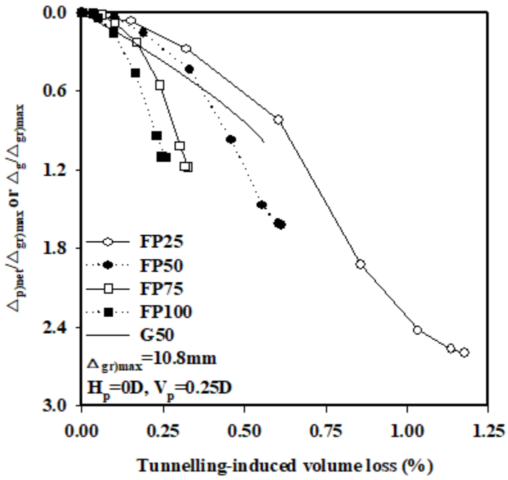

Fig. 7 Distributions of normalised tunnelling-induced pile head and greenfield soil surface settlements with the tunnelling-induced volume loss at Y/D=3.5

respectively. To analyse the behaviour of existing piles in response to tunnelling, the allowable pile forces were applied on the pile head prior to tunnelling.

3.2 Settlement of the ground and piles

Table 3 presents the normalised tunnelling-induced maximum pile head settlements ($\Delta_{p,net)max}/\Delta_{gr)max}$) and the normalised tunnelling-induced maximum axial pile forces ($P_{net)max}/P_a$) for various pile tip locations and the face pressures, where $\Delta_{p,net)max}$ is the maximum tunnelling-induced pile head settlement; $\Delta_{gr)max}$ is the maximum soil surface settlement at the centre of a pile with H_p=0, which is computed from the FP50 greenfield condition; and $P_{net)max}$ is the tensile or compressive force. The largest pile head settlement developed with the smallest tunnel face pressure, and all the piles with the tips in the upper part of the tunnel crown (H_p=0) developed tensile pile forces regardless of the face pressures. This will be discussed in detail later.

Fig. 6(a) shows the changes in the normalised tunnelling-induced pile head settlements $\Delta_{p)net}/\Delta_{gr)max}$ and the soil surface settlements $\Delta_g/\Delta_{gr)max}$ for all tunnel excavation steps (X/D = 0D ~ +7D) for the FP50 condition with various pile tip locations (V_p=0.25D, 0.5D, 0.75D and 1D) and with H_p=0D, where $\Delta_{p)net}$ is the tunnelling-induced pile head settlement, which excludes the pile settlement that developed under the application of the axial pile loading; Δ_g is the soil surface settlement at the pile centre location, which is obtained from the greenfield condition; and $\Delta_{gr)max}$ is the maximum soil surface settlement at the centre pile location, which is computed from the FP50 greenfield condition ($\Delta_{gr)max}$ =10.8 mm). According to Fig. 6(a), $\Delta_{p)net}/\Delta_{gr)max}$ and $\Delta_g/\Delta_{gr)max}$ increased as the tunnel excavation proceeded. The rate of the pile settlement increase at each analysis step was maximal when tunnelling was conducted at Y/D =±1 from the pile location (behind and ahead of the pile axis in the longitudinal direction) and approximately 69% of $\Delta_{p,net)max}$ had developed, where $\Delta_{p,net)max}$ is the maximum tunnelling-induced pile head settlement. This occurred when the tunnel face was located below the pile axis (Y/D = 3.5). Subsequently, the rate of the settlement was observed to be significantly reduced. Additionally, when the tunnelling was conducted at ±0.5D from the pile centre in the longitudinal direction, approximately 37% of $\Delta_{p,net)max}$ was realised. All the piles in most of the tunnel excavation are analysed to exceed the surface settlement of the greenfield condition. At the end of the tunnel excavation, the pile head settlement at the shortest vertical distance from the tunnel FP50(V_p=0.25D) was $\Delta_{p)net}/\Delta_{gr)max}$ = 1.62. As the vertical distance of the pile tip from the tunnel increased (V_p=0.5D-1D), the pile head settlements gradually decreased to $\Delta_{p)net}/\Delta_{gr)max}$ = 1.41, 1.27 and 1.18. The pile head settlement at the end of the tunnel excavation, namely, FP50(V_p=1D), was reduced by 27% compared to FP50(V_p=0.25D) because the ground settlements decreased towards the surface from the tunnel.

Fig. 6(b) shows changes in the normalised tunnelling-induced pile head settlement $\Delta_{p)net}/\Delta_{gr)max}$ and the soil surface settlement $\Delta_g/\Delta_{gr)max}$ for all tunnel excavation steps

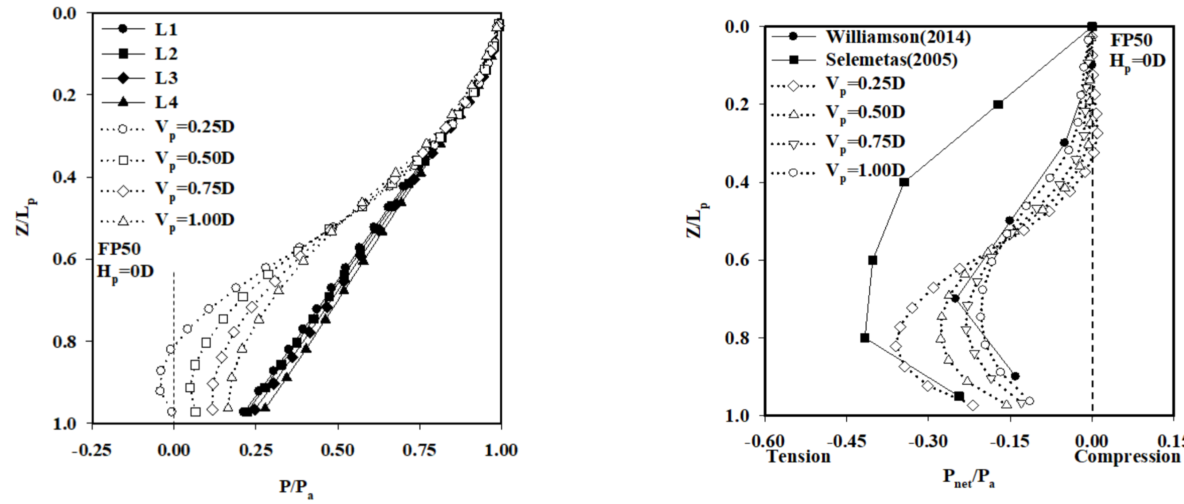

(a) (b)

Fig. 8 (a) Distributions of normalised axial pile forces with the depth (H_p=0D and FP50) and (b) Distributions of normalised tunnelling-induced axial pile forces with the depth (H_p=0D and FP50)

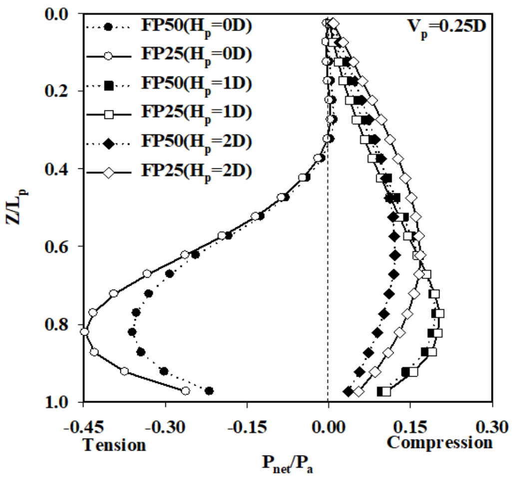

Fig. 9 Distributions of normalised tunnelling-induced axial pile forces with the depth (V_p=0.25D and L_p=20 m)

(Y/D = 0D ~ +7D) by considering FP50 and FP25 according to the various horizontal distances (H_p=0D, 1D and 2D) with location V_p=0.25D (L_p=20 m), where $\Delta_{p)net}$ is the tunnelling-induced pile head settlement that excludes the pile settlement that developed under application of the axial pile loading and $\Delta_{gr)max}$ is the maximum soil surface settlement at the location of the centre pile (H_p=0D), which was computed from the FP50 greenfield condition ($\Delta_{gr)max}$=10.8 mm). The pile head settlements at the end tunnel excavation for FP50(H_p=0D) and FP25(H_p=0D) are significantly larger than the pile head settlements under other conditions due to existing piles above the tunnel crown. Additionally, the pile head settlement at the end tunnel excavation of FP25(H_p=0D) was computed as approximately 1.6 times larger than that of FP50(H_p=0D) and approximately 11 times larger than that of FP50(H_p=2D). The pile settlement for FP25(H_p=1D) was larger than that for FP50(H_p=0D) until Y/D=0.00~3.45, and, subsequently, the final pile head settlement was small. It has been shown that the tunnel excavation causes ground settlements that differ according to the face pressure conditions; hence, comparison with the tunnel influence zone may be necessary.

Fig. 7 plots the normalised pile heads $\Delta_{p)net}/\Delta_{gr)max}$ and the free-field ground surface settlements $\Delta_g/\Delta_{gr)max}$ with tunnelling-induced volume losses at Y/D=3.5 for the various face pressure conditions with the pile tip location of V_p=0.25D and H_p=0D. Under the greenfield condition, the soil surface settlement increases with the volume loss almost linearly; however, when there was a pile in the ground, the pile settlements increased rapidly. Additionally, as the magnitude of the tunnel face pressure decreased, the volume losses and the pile settlements increased, as shown in Fig. 7. Under the FP25 condition, the volume loss after the completion of tunnelling was approximately 1.2%, and the pile settlement according to the volume loss was the largest. In contrast, under the FP75 and FP100 conditions, the volume losses after the completion of tunnelling were less than 0.5%.

3.3 Distributions of the axial pile forces

Fig. 8(a) presents the distributions of the normalised axial pile forces P/P_a with the normalised pile depth (Z/L_p) for FP50 at four pile tip locations (V_p=0.25D, 0.5D, 0.75D and 1D, with H_p=0D), where P is the axial pile force at a specified depth and P_a is the service pile load prior to tunnelling. The axial pile forces that are due to pile loading on the head prior to tunnel excavation and the axial pile force distributions upon completion of tunnelling are shown in Fig. 8(a). The distributions of the normalised axial pile forces according to the design load (L1~L4) were similar for all the piles, and the axial pile forces near the pile tip were P/P_a = 0.20~0.28. In contrast, upon completion of the tunnel excavation, the axial pile forces of the pile tips are decreased by the tunnelling-induced positive shaft resistance. In the case of the V_p=0.25D pile, small tensile pile forces (maximum P/P_a = -0.04) were computed at Z/L_p = 0.8~1.0. However, the structural problem of the pile has

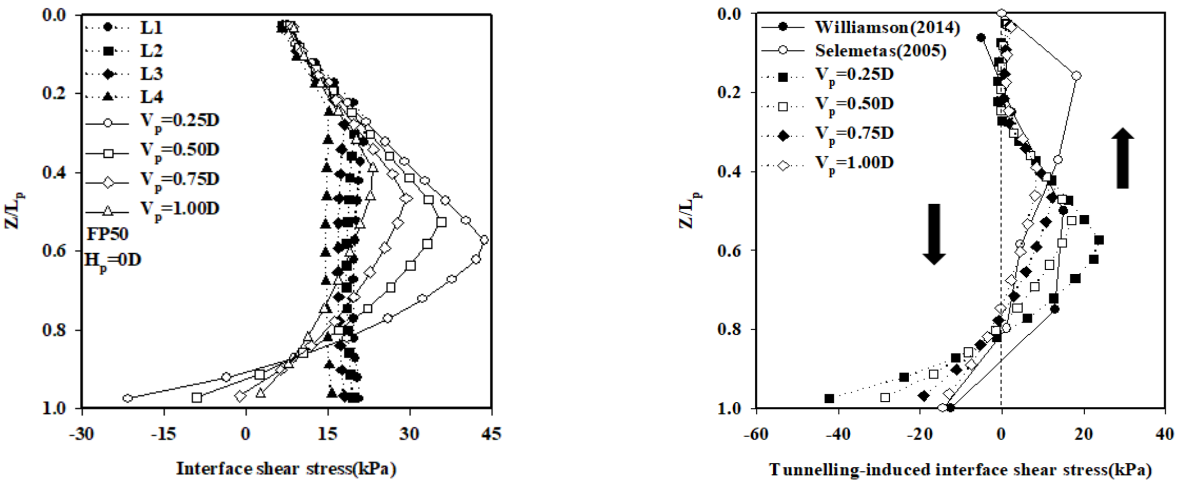

(a) (b)

Fig. 10 (a) Distributions of the interface shear stresses with the depth (H_p=0D and FP50) and (b) Distributions of the tunnelling-induced interface shear stresses with the depth (H_p=0D and FP50)

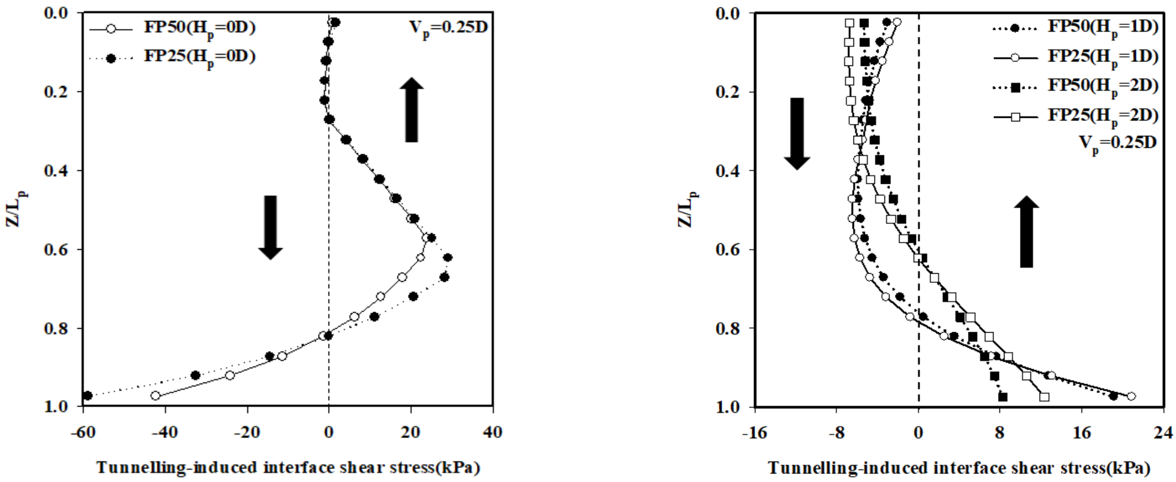

(a) Distributions of the tunnelling-induced interface shear stresses (H_p=0D)

(b) Distributions of the tunnelling-induced interface shear stresses (H_p=1D and 2D)

Fig. 11 Distributions of the tunnelling-induced interface shear stresses with the depth (V_p=0.25D and L_p=20 m)

been unlikely to develop because these forces are very small compared to the typical allowable tensile strength of the pile material.

Fig. 8(b) presents the distribution of the normalised tunnelling-induced axial pile forces P_{net}/P_a with the normalised pile depth (Z/L_p) to clarify the effects of tunnelling on the axial pile forces for FP50 at the various pile tip locations (V_p=0.25D, 0.5D, 0.75D and 1D) with H_p=0D, where P_{net} is the tunnelling-induced axial pile force. Additionally, the axial pile forces of all pile conditions decreased from the surface to near Z/L_p = 0.8, and $P_{net)(-)max}/P_a$ values of -0.36 and -0.20 are computed for the piles of FP50(V_p=0.25D) and FP50(V_p=1.00D), respectively, where $P_{net)(-)max}$ is the maximum tensile pile force. According to these results, as the vertical distances of the pile tips from the tunnel crown increased, the maximum values of the tensile force decreased. Fig. 8(b) plots the normalised tunnelling-induced axial pile force distributions that are deduced from a field measurement and a geotechnical centrifuge test that were reported by Selemetas (2005) and Williamson (2014), respectively, for comparison. The $P_{net)(-)max}/P_a$ values of -0.42 and -0.25 were obtained based on studies that were reported by Selemetas (2005) and Williamson (2014), respectively. The distributions of the tunnelling-induced tensile pile forces that were deduced from these works agree with the computed results, which supports the validity of the current results.

Fig. 9 shows the distribution of the normalised tunnelling-induced axial pile force P_{net}/P_a with the normalised pile depth (Z/L_p) that is obtained by considering FP50 and FP25 with various horizontal distances of the pile tips from the tunnel (H_p=0D, 1D and 2D, and V_p=0.25D (L_p=20 m)). The tunnelling-induced tensile pile forces were computed for FP50(H_p=0D) and FP25(H_p=0D) above the tunnel crown; however, other piles with H_p=1D and 2D that were measured from the tunnel centre were subjected to compressive pile forces, as shown in Fig. 9. The distributions of the axial pile forces depend heavily on the pile tip location. The axial pile forces for H_p=0D and 2D with FP25 were observed to be larger than the those with FP50. This was anticipated due to the high degree of shear strength mobilisation between the pile and the soil since a lower face pressure corresponds to larger ground settlements. The maximum tensile pile force of P_{net}/P_a = -0.45 in FP25(H_p=0D) was computed (inside the influence zone), and the maximum compressive pile force P_{net}/P_a = 0.2 in FP25(H_p=1D) was obtained (outside the influence zone and on the boundary). Therefore, it is concluded that sufficient consideration of the magnitudes of the face pressures is required because the change in the face pressure has significant effects on the ground settlements and the pile settlements.

3.4 Shear stresses at the interface

Fig. 10(a) shows the distributions of the shear stresses at the pile-soil interface with the normalised pile depth (Z/L_p) for FP50 at the various vertical distances (V_p=0.25D, 0.5D, 0.75D and 1D, with H_p=0D) and excluding the effect of the axial pile loading prior to tunnelling. The distributions of the shear stress under the design loading were similar; however, the longer the pile length, the larger the shear stresses. Under the pile loading, the shear stresses are fully mobilised from the pile head to approximately Z/L_p=0.3, after which only slight changes of the shear stresses are computed. However, the ranges of plastic soil yielding at the pile-soil interface are expanded due to tunnelling: The closer the pile tip to the tunnel, the larger the range of the soil yielding. There are points where the depth of the shear stress changes from (+)ve to (-)ve, namely, the directions of the shear stress components change from upward to downward, as reported by Lee (2012). The shear stresses after the completion of tunnelling were increased to Z/L_p=0.57 in FP50(V_p=0.25D), after which the shear stresses gradually was decreased to the (-)ve value. Additionally, the shear stresses under other conditions increased to Z/L_p=0.39-0.53 after the completion of tunnelling but gradually decreased towards the pile tip. Thus, the shear strength was completely mobilised from the pile head to the specified depth, and only part of the shear strength was mobilised below the specified depth.

Fig. 10(b) presents the distributions of the tunnelling-induced shear stresses at the pile-soil interface with the normalised pile depth (Z/L_p) for FP50 at the various vertical distances (V_p=0.25D, 0.5D, 0.75D and 1D, with H_p=0D). The piles of all conditions developed very small shear stresses from the pile head to near Z/L_p= 0.30 due to the full mobilisation of skin frictions in response to the pile loading, as explained above, which corresponds to the development of soil slip. In the case of FP50(V_p=0.25D), the shear stress gradually increased from Z/L_p=0.30 to 0.57 where the maximum shear stress was computed. Then, the shear stress below Z/L_p=0.57 decreased towards the (-)ve values at the pile tip. Similar trends were observed in the piles under other conditions. Fig. 10(b) also shows the normalised tunnelling-induced interface shear stress distributions that were deduced from previous studies by Selemetas (2005) and Williamson (2014). The computed shear stress distribution deviates slightly from the measurements; however, the trend of the distributions of the shear stresses are qualitatively similar.

Figs. 11(a) and 11(b) show the distributions of the tunnelling-induced shear stresses at the pile-soil interface with the normalised pile depth (Z/L_p) under conditions FP50 and FP25 for various pile tip positions (H_p=0D, 1D and 2D, and V_p=0.25D (L_p=20 m)). In the cases of FP50(H_p=0D) and FP25(H_p=0D), upward (resisting) shear stress at the upper end of the pile and downward (acting) shear stress at the lower end of the pile were computed as indicated by the arrows in the figures. The smaller face pressure causes the ground settlements to increase, and the relative displacements between the pile and the soil increase; hence, the shear stresses increase. Therefore, in the case of FP25(H_p=0D), the maximum positive shear stress was larger and the minimum negative shear stress was smaller compared to those that were computed for FP50(H_p=0D). For the piles outside the influence zone and on the boundary [with FP50(H_p=1D), FP25(H_p=1D), FP50(H_p=2D) and FP25(H_p=2D)], opposite shear stress distributions with smaller magnitudes are obtained. A small downward (acting) shear stress at the upper end of the pile and a relatively large upward (resisting) shear stress at the lower end of the pile developed. Hence, the upper part of the soil drags the pile down, while lower part of the soil resists pile settlement, thereby resulting in compression of the pile, as explained in Section 3.3.

3.5 Relative shear displacements at the interface

Fig. 12 shows the distributions of the relative shear displacements at the pile-soil interface with the normalised pile depth (Z/L_p) that are obtained by considering two face pressures, namely, FP25 and FP50, with various horizontal distances of the pile tips (H_p=0D, 1D and 2D; V_p=0.25D; and L_p=20 m). Prior to tunnel excavation, the pile settlement was larger than the soil settlement over the entire pile depth under the application of the axial pile loading, which mobilised positive shaft resistance at the interface, as expected. However, after the tunnel excavation was completed at H_p=0D, the relative displacements increased substantially. In contrast, in the cases of H_p=1D and 2D, substantially smaller relative displacements developed compared with the H_p=0D condition. In addition, the distributions of the relative displacements for each analysis are not consistent; hence, it may be necessary to consider tunnelling-induced relative shear displacements in detail.

Figs. 13(a) and 13(b) present the distributions of the tunnelling-induced relative shear displacements (pile movement-soil movement) at the pile-soil interface with the normalised pile depth for two face pressures, namely, FP25 and FP50, with various pile tip locations (H_p=0D, 1D and 2D; V_p=0.25D; and L_p=20 m). Under the FP25 condition, the relative shear displacements are computed to be relatively large compared with the FP50 condition, which causes larger shear stresses. The tunnelling-induced pile settlements ($\triangle_{pile}$) for the H_p=0D condition are larger than the tunnelling-induced soil settlements ($\triangle_{soil}$) at the upper part of the pile (Z/L_p= 0.0 ~ 0.8), whereas at the lower parts of the piles (Z/L_p= 0.0 ~ 1.0), the relative displacements

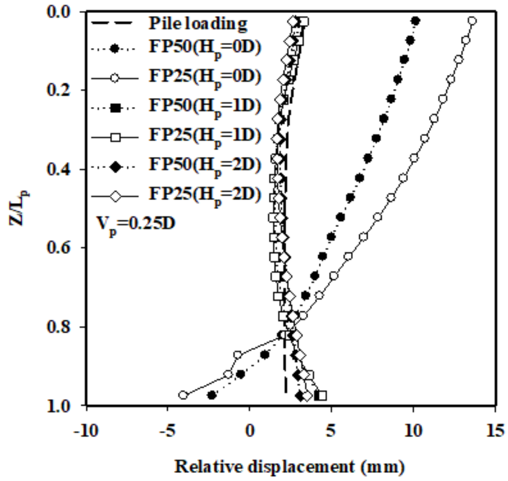

Fig. 12 Distributions of the relative displacements with the depth(V_p=0.25D and L_p=20 m)

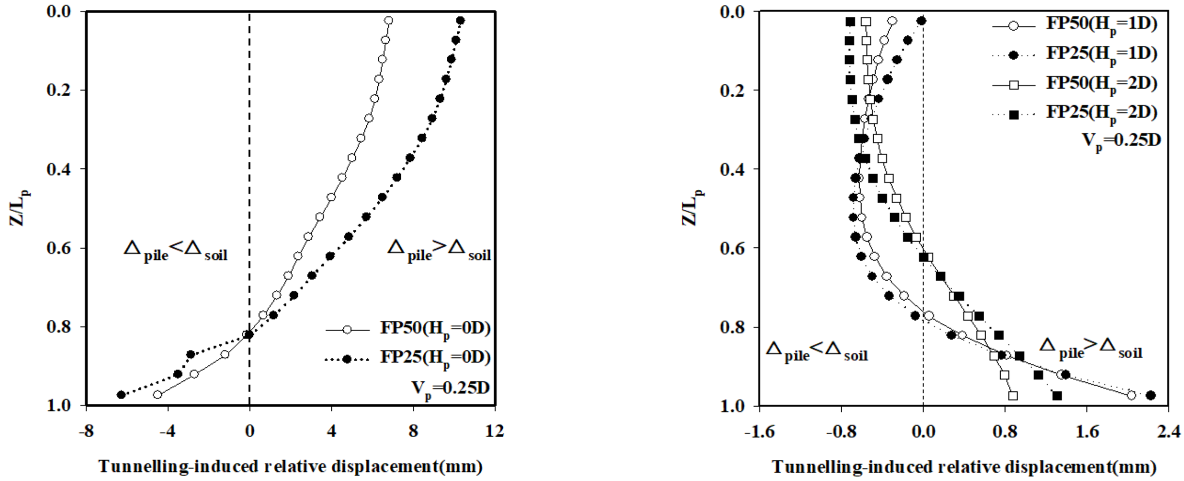

(a) Distributions of the tunnelling-induced relative displacements (H_p=0D)

(b) Distributions of the tunnelling-induced relative displacements (H_p=1D, 2D)

Fig. 13 Distributions of the tunnelling-induced relative displacements at the pile-soil interface with the depth (V_p=0.25D and L_p=20 m)($\triangle_{pile}$: tunnelling-induced pile settlements and $\triangle_{soil}$: tunnelling-induced soil settlements at the pile-soil interface)

gradually decrease, which probably resulting from downward movement of the soil near the tunnel ($\triangle_{soil} > \triangle_{pile}$). Therefore, the upper parts of the piles mobilised to restrain the pile movements that were triggered by ground settlement that was caused by the tunnelling. Hence, the shear stress distributions that are presented above are supported by the relative shear displacements. This trend is consistent with the distributions of the shear stresses, thereby implying upward (resisting) shear stress at the upper end of the pile and downward (acting) shear stress at the lower part of the pile when the piles are inside the influence zone. However, the distributions of the relative displacements when the piles are outside the influence zone and on the boundary (H_p=1D and 2D) are opposite, thereby resulting in compression of the piles, as explained previously.

Fig. 14(a) presents the distributions of the effective normal stresses at the pile-soil interface for the two face pressures of FP25 and FP50 with various horizontal distances of the pile tips (H_p=0D, 1D and 2D; V_p=0.25D; and L_p=20 m) versus the normalised pile depth(Z/L_p). Except for the piles at the upper part of the tunnel crown, all the piles under the axial pile loading and tunnelling developed similar normal stresses. In contrast, for the piles (H_p=0D) on the upper part of the tunnel crown, the normal stress distributions were smaller than that of the pile of the service loading. This is because the settlements of the surrounding soil at the pile were larger than under the other conditions (H_p=1D and 2D). Under the H_p=0D condition, as the depth of the pile increased, the settlements of the surrounding soil at the pile increased due to tunnelling and, hence, the normal stresses decreased. For this reason, it may be necessary to examine the tunnelling-induced normal stress distributions of the surrounding soil with the pile depth.

Fig. 14(b) shows the distributions of the tunnelling-

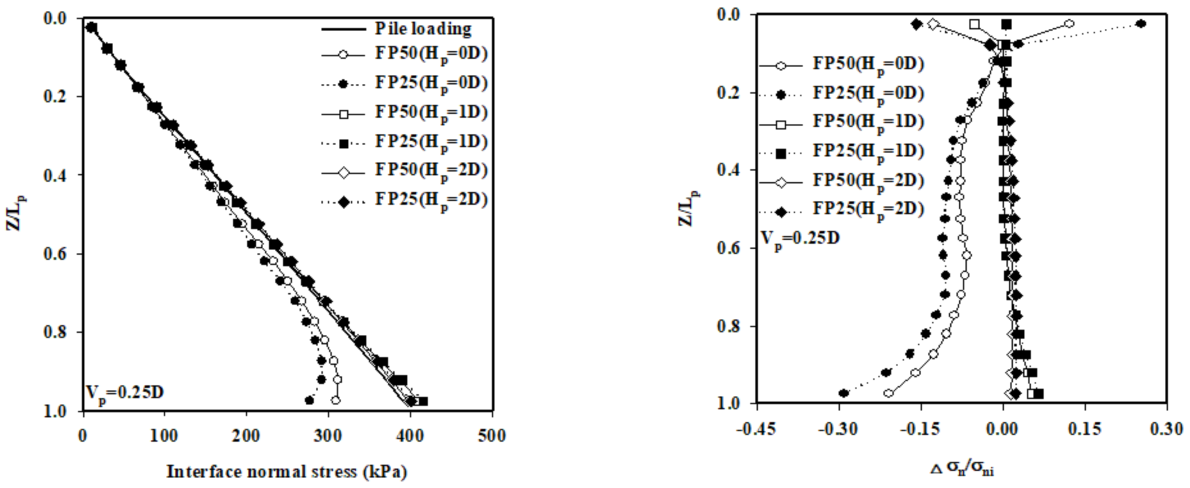

(a) (b)

Fig. 14 (a) Distributions of the interface normal stresses with the depth (V_p=0.25D) and (b) Distributions of the normalised tunnelling-induced interface normal stresses with the depth (V_p=0.25D)

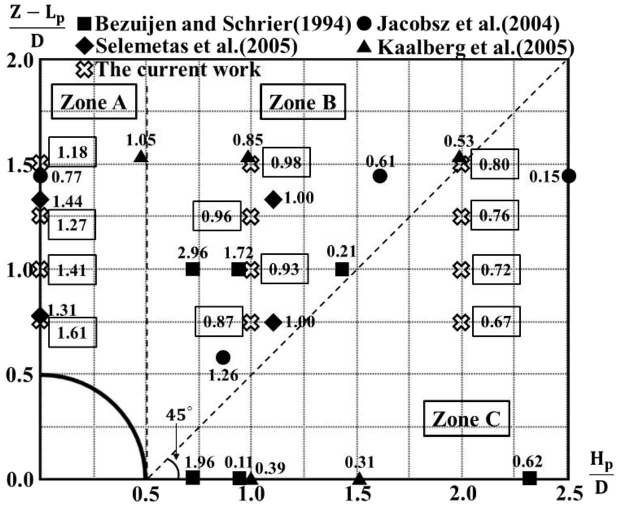

Fig. 15 Tunnelling-induced pile/surface settlement ratios ($\triangle_{p)net}/\triangle_{surf)max,net}$) for various pile tip locations that were calculated in the current work and reported in the literature (Dias and Bezuijen 2014b)

induced normalized effective normal stresses $\triangle\sigma_n/\sigma_{ni}$ at the interface for two face pressures, namely, FP25 and FP50, with various horizontal distances of the pile tips (H_p=0D, 1D and 2D; V_p=0.25D; and L_p=20 m) versus the normalised pile depth (Z/L_p), where $\triangle\sigma_n$ is the change in the normal stresses due to tunnelling and σ_{ni} is the initial normal stress prior to the application of the axial pile loading. The normalised normal stress along the direction of increase of the pile depth at H_p=0D is greater than the stresses at H_p=1D and 2D. Under the H_p=0D condition, from the pile head to Z/L = 0.8, the normal stresses are increased by approximately 30~40%, while much larger increases are computed near the pile base (Z/L = 0.8~1.0). The normalised normal stresses near the pile tip are larger than the initial normal stress due to soil arching and dilation, as discussed by Jacobsz (2003). In contrast, under the H_p=2D condition, the normal stresses increased slightly near the pile tip; this is because the surrounding soil near the pile tip may constrain the pile movement more than under the H_p=0D condition.

3.6 Analysis of the pile behaviour by considering previous studies

Fig. 15 shows the ratios ($\triangle_{p)net}/\triangle_{surf)max,net}$) of the tunnelling-induced pile settlement ($\triangle_{p)net}$) to the maximum tunnelling-induced ground surface settlement ($\triangle_{surf)max,net}$) with respect to the normalised depth ((Z-L_p)/D) and normalised horizontal distance (H_p/D) of the pile tips, which are obtained by considering the results of previous studies that are summarised by Dias and Bezuijen (2014b) and the current work, where Z is the distance from the surface to the tunnel centre, and L_p, H_p and D are marked on the layout of Fig. 3(a). Additionally, the values that were obtained via the numerical analysis that was conducted in the current study are represented by boxes. The piles for H_p/D values between 0.0 and 0.5 were larger than 1, except for the value of 0.77 that was proposed by Jacobsz *et al.* (2004), and these results are similar to the results of the numerical analysis that was conducted in the current study. For H_p/D of 0.5 ~ 1.5, the values of $\triangle_{p)net}/\triangle_{surf)max}$, net were distributed at approximately 1. The piles at horizontal distances in excess of 1.5 from the tunnel were less than 1 in both the previous studies and the numerical analysis of the current work. If the value of $\triangle_{p)net}/\triangle_{surf)max,net}$ exceeds 1, the pile head settlements exceed the surface settlements, whereas if the value of $\triangle_{p)net}/\triangle_{surf)max,net}$ is less than 1, the reverse trend is observed. Fig. 15 also shows three zones that were proposed by Selemetas *et al.* (2005). Selemetas *et al.* (2005) discussed this relation by proposing three zones, namely, zones A~C, around the tunnel. In summary, piles with bases in Zone A were shown to settle 2~4 mm more than the ground surface (R > 1, where R is $\triangle_{p)net}/\triangle_{surf)max,net}$). Piles with their bases in Zone B (defined by an angle of 45° between Zones A and C, as shown in Fig. 15) settled by the same amount as the surface (R = 1). Finally, piles with their bases in Zone C were found to settle less than the surface (R < 1). The computed tunnelling-

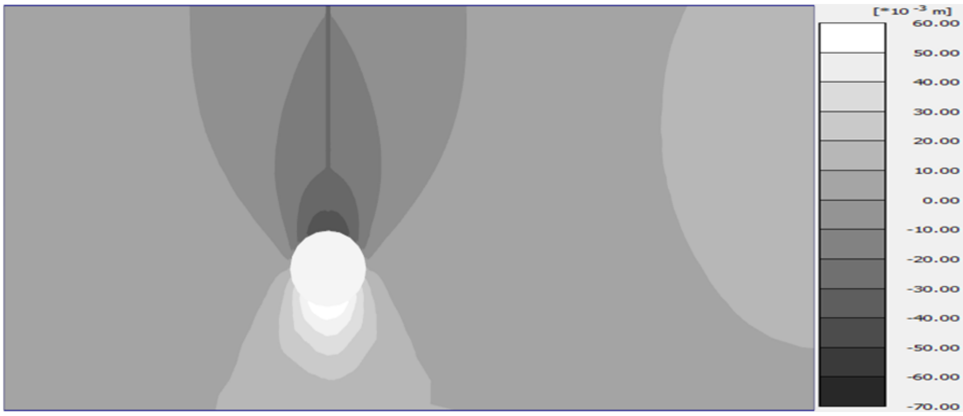

(a) FP25($\triangle_p$: 33.6 mm, $\triangle_{surf)max}$: 19.7 mm)

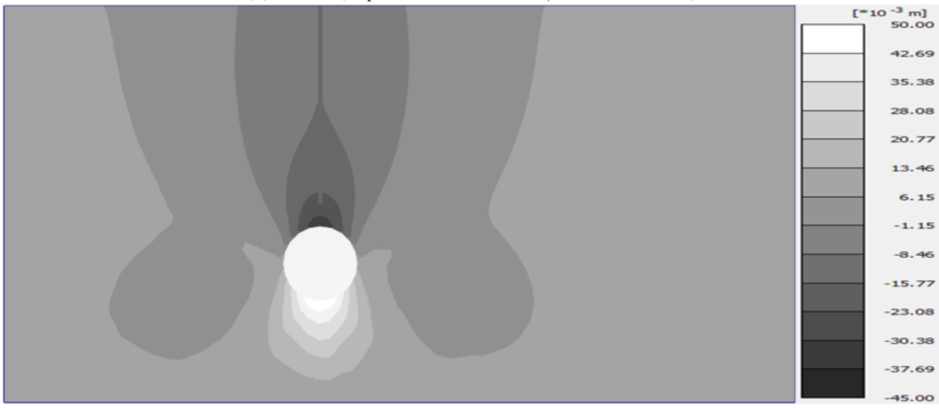

(b) FP50($\triangle_p$: 22.8 mm, $\triangle_{surf)max}$: 12.4 mm)

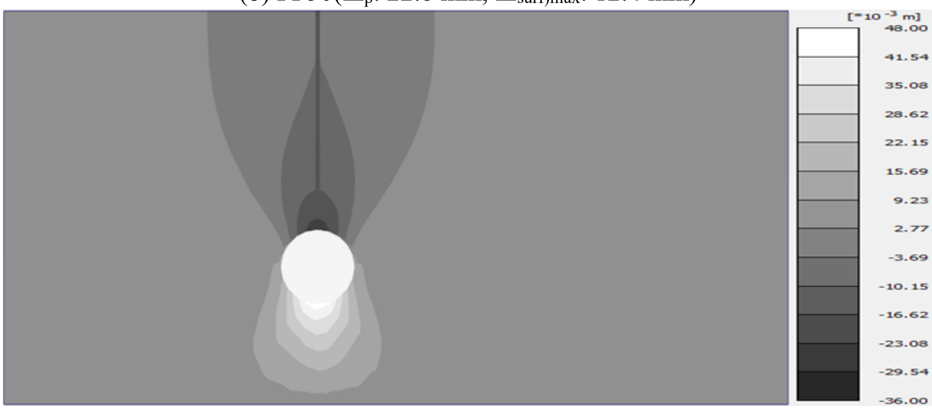

(c) FP75($\triangle_p$: 17.8 mm, $\triangle_{surf)max}$: 8.9 mm)

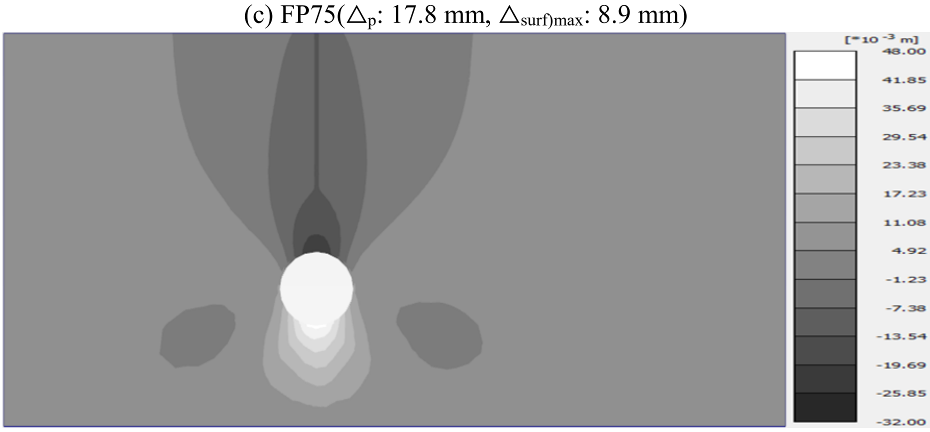

(d) FP100($\triangle_p$: 16.9 mm, $\triangle_{surf)max}$: 8.2 mm)

Fig. 16 Pile and ground settlements for various face pressures (X-Z plane; Y/D=3.5 (pile tips are above the tunnel crown), H_p=0D, and V_p=0.25D)[$\triangle_p$: pile head settlement and $\triangle_{surf)max}$: maximum surface settlement] induced settlements of the piles in Zone A in the current study were similar or slightly larger than those that were estimated by Selemetas *et al.* (2005). Similarly, the tunnelling-induced pile settlements in Zones B and C are also consistent with those of Selemetas *et al.* (2005).

3.7 Settlement contours according to the changes in the face pressures

Figs. 16(a)-16(d) plot the settlement contours of the pile and the ground according to various face pressures upon completion of tunnelling at Y/D=3.5 on the X-Z plane(pile tips are directly above the tunnel crown). The pile settlements and the ground settlements include all the movements that are associated with the pile loading and tunnelling. Fig. 16(a) plots the contour for the FP(25) condition. The settlement at the upper part of the tunnel crown was approximately 50 mm, and the settlement at the surface was approximately 20 mm. According to the analysis, the pile settlements and the ground settlements increased due to the decreasing the face pressure. Furthermore, the difference in the settlements between the pile and the ground also increased. Fig. 16(d) plots the contour for the largest face pressure (FP(100)). Under the FP(100) condition, the pile settlement was roughly 17 mm, and the surface settlement was about 8 mm. The settlement characteristics of the pile and the ground differ according to the magnitude of the face pressure, and the influences of the face pressure were adequately expressed by the contour lines.

4. Conclusions

A series of three-dimensional parametric numerical analyses were conducted to study the responses of the piles to adjacent shield tunnelling while considering two key factors: the face pressures and the relative pile tip locations. The following conclusions are drawn from the present study regarding the pile head settlements, the axial pile forces, the interface shear stresses and the relative shear displacements.

• When the pile tips are directly above the tunnel crown, pile head settlements that exceed the surface settlements of the greenfield conditions have developed. The rate of pile settlement increased at each analysis step, and the maximum value was attained when tunnelling was conducted at Y/D=±1.0 behind and ahead of the pile axis in the longitudinal direction from the pile centre, where approximately 69% of the final settlement had developed when tunnelling underneath the pile tip. The pile head settlement when the face pressure was 25% of the in situ horizontal soil stress (FP25) was computed to be approximately 1.6 times larger than that computed for the face pressure of 50% of the in situ horizontal soil stress (FP50) for the piles above the tunnel crown. In addition, the smallest pile settlements developed at the farthest pile from the tunnel, which were only approximately 10% of the largest pile settlement when the pile tip was above the tunnel crown with the minimum vertical distance between the pile tip and the tunnel crown.

• For the piles above the tunnel crown, the tunnelling-induced tensile pile forces decreased with the pile depth, which was consistent with previous studies from field measurements. The maximum normalised tensile pile force, namely, P_{net}/P_a = -0.45, was computed with FP25 for the pile inside the tunnel influence zone; also, the maximum normalised compressive pile force, namely, P_{net}/P_a = 0.20, was obtained with FP25 for the pile outside the tunnel influence zone. It has been demonstrated that the pile behaviour depends heavily on the locations of pile tips with respect to the tunnel position.

• For the piles inside the influence zone, an upward (resisting) shear stress at the upper end of the pile and a downward (acting) shear stress at the lower end of the pile developed. In contrast, for the piles outside the influence zone and on the boundary, a small downward (acting) shear stress at the upper end of the pile and a relatively large upward (resisting) shear stress at the lower end of the pile developed. The relative shear displacements with the face pressure of 25% of the in situ horizontal soil stress are computed to be relatively large compared with those with the face pressure of 50%,75% and 100% of the in situ horizontal soil stress; the same result is obtained for the shear stresses.

• In the current study, a comparative analysis was conducted based on previous studies from the literature. The ratio of the tunnelling-induced pile head settlement to the surface settlement ($\triangle_{p)net}/\triangle_{surf)max,net}$) inside the tunnel influence zone was larger than 1 or about 1. In contrast, for the piles outside the tunnel influence zone, the value of ($\triangle_{p)net}/\triangle_{surf)max,net}$) was calculated to be less than 1 in both the previous studies and the current study. Hence, the computed results of the previous study and the current study were similar for the tunnel influence zone, which supports the validity of the current study. It is anticipated that the tunneling influence zone may be used to assess pile response to adjacent tunnelling and to estimate tunnelling-induced pile settlements.

Acknowledgments

This research was supported by Basic Science Research Program through the National Research Foundation of Korea(NRF) funded by the Ministry of Education(2017R1D1A1B05035579).

References

Ahn, C.K., Yu, J.S. and Lee, S.W. (2018), "Evaluation of the backfill injection pressure and its effect on ground settlement for shield TBM using numerical analysis", *J. Kor. Tunn. Undergr. Sp. Assoc.*, **20**(2), 269-286. https://doi.org/10.9711/KTAJ.2018.20.2.269.

Bezuijen, A. and van der Schrier, J.S. (1994), "The influence of a bored tunnel on pile foundations", *Proceedings of the International Conference Centrifuge 94*, Singapore, August-September.

Bolton, M.D. (1991), *A Guide to Soil Mechanics*, M.D. & K. Bolton, Cambridge, 313.

Brinkgreve, R.B.J., Kumarswamy, S. and Swolfs, W.M. (2015), *Reference Manual*, in *Plaxis 3D 2015 User's Manual*, Delft, The Netherlands, 1-284.

Cheng, C.Y., Dasari, G.R., Chow, Y.K. and Leung, C.F. (2007), "Finite element analysis of tunnel-soil-pile interaction using displacement controlled model", *Tunn. Undergr. Sp. Technol.*, **22**(4), 450-466. https://doi.org/10.1016/j.tust.2006.08.002.

Cho, W.S., Song, K.I. and Kim, K.Y. (2014b), "The study on the effect of fracture zone and its orientation on the behaviour of shield TBM cable tunnel", *J. Kor. Tunn. Undergr. Sp. Assoc.*, **16**(4), 403-415. https://doi.org/10.9711/KTAJ.2014.16.4.403.

Cho, W.S., Song, K.I. and Ryu, H.H. (2014a), "Analysis on the behaviour of shield TBM cable tunnel: The effect of the distance of backfill grout injection from the end of skin plate", *J. Kor. Tunn. Undergr. Sp. Assoc.*, **16**(2), 213-224. https://doi.org/10.9711/KTAJ.2014.16.2.213.

Davisson, M.T. (1972), "High capacity piles", *Proceedings of the Lecture Series in Innovations in Foundation Construction*, Illinois Section, ASCE.

Dias, T.G.S. and Bezuijen, A. (2014a), "Pile tunnel interaction: Literature review and data analysis", *Proceedings of the ITA World Tunnel Congress 2014*, Iguassu Falls, Brazil, May.

Dias, T.G.S. and Bezuijen, A. (2014b), "Pile-tunnel interaction: A conceptual analysis", *Proceedings of the 8th International Symposium on Geotechnical Aspects of Underground Construction in Soft Ground*, Seoul, Korea, August.

Hartono, E., Leung, C.F., Shen, R.F., Chow, Y.K., Ng, Y.S., Tan, H.T. and Hua, C.J. (2014), "Behaviour of pile above tunnel in clay", *Proceedings of the 8th International Conference on Physical Modelling in Geotechnics*, Perth, Australia, January.

Jacobsz, S.W. (2002), "The effects of tunnelling on piled foundations", Ph.D. Thesis, University of Cambridge, Cambridge, U.K.

Jacobsz, S.W. (2003), "Tunnelling effects on piled foundations", *Tunn. Tunn. Int.*, **35**(6), 28-31.

Jacobsz, S.W., Standing, J.R., Mair, R.J., Soga, K., Hagiwara,T. and Sugiyama, T. (2004), "Centrifuge modelling of tunnelling near driven piles", *Soils Found.*, **44**(1), 51-58. https://doi.org/10.3208/sandf.44.49.

Kaalberg, F.J., Teunissen, E.A.H., van Tol, A.F. and Bosch, J.W. (2005), "Dutch research on the impact of shield tunnelling on pile foundations", *Proceedings of the 5th International Conference of TC 28 of the ISSMGE, Geotechnical Aspects of Underground Construction in Soft Ground*, London, U.K., June.

Lee, C.J. (2012), "Three-dimensional numerical analyses of the response of a single pile and pile groups to tunnelling in weak weathered rock", *Tunn. Undergr. Sp. Technol.*, **32**, 132-142. https://doi.org/10.1016/j.tust.2012.06.005.

Lee, C.J. (2013), "Numerical analysis of pile response to open face tunnelling in stiff clay", *Comput. Geotech.*, **51**, 116-127. https://doi.org/10.1016/j.compgeo.2013.02.007.

Lee, C.J. and Chiang, K.H. (2007), "Responses of single piles to tunnelling-induced soil movements in sandy ground", *Can. Geotech. J.*, **44**(10), 1224-1241. https://doi.org/10.1139/T07-050.

Lee, C.J., Jeon, Y.J., Kim, S.H and Park, I.J. (2016), "The influence of tunnelling on the behaviour of pre-existing piled foundations in weathered soil", *Geomech. Eng.*, **11**(4), 553-570. https://doi.org/10.12989/gae.2016.11.4.553.

Lee, G.T.K. and Ng, C.W.W. (2005), "The effects of advancing open face tunnelling on an existing loaded pile", *J. Geotech. Geoenviron. Eng.*, **131**(2), 193-201. https://doi.org/10.1061/(ASCE)1090-0241(2005)131:2(193).

Lee, J.H., Lee, J.M. and Lee, Y.J. (2012), "Behaviour of the superstructure subjected to TBM tunnel excavation sequence", *Proceedings of the KSCE 2017 Convention Conference & Civil EXPO*, Busan, Korea, October.

Lee, Y.J. (2016), "Determination of tunnel support pressure under the pile tip using upper and lower bounds with a superimposed approach", *Geomech. Eng.*, **11**(4), 587-605. https://doi.org/10.12989/gae.2016.11.4.587.

Liu, C., Zhang, Z. and Regueiro, R.A. (2014), "Pile and pile group response to tunnelling using a large diameter slurry shield – Case study in Shanghai", *Comput. Geotech.*, **59**, 21-43. https://doi.org/10.1016/j.compgeo.2014.03.006.

Mair, R.J. and Williamson, M.G. (2014), "The influence of tunnelling and deep excavation on piled foundations", *Proceedings of the 8th International Symposium on Geotechnical Aspects of Underground Construction in Soft Ground*, Seoul, Korea, August.

Marshall, A.M. (2009), "Tunnelling in sand and its effect on pipelines and piles", Ph.D. Thesis, University of Cambridge, Cambridge, U.K.

Mroueh, H. and Shahrour, I. (2008), "A simplified 3D model for tunnel construction using tunnel boring machines", *Tunn. Undergr. Sp. Technol.*, **23**, 38-45. https://doi.org/10.1016/j.tust.2006.11.008.

Ng, C.W.W. and Lu, H. (2014), "Effects of the construction sequence of twin tunnels at different depths on an existing pile", *Can. Geotech. J.*, **51**(2), 173-183. https://doi.org/10.1139/cgj-2012-0452.

Ng, C.W.W., Lu, H. and Peng, S.Y. (2013), "Three-dimensional centrifuge modelling of twin tunnelling effects on an existing pile", *Tunn. Undergr. Sp. Technol.*, **35**, 189-199. https://doi.org/10.1016/j.tust.2012.07.008.

Ng, C.W.W., Soomro, M.A. and Hong, Y. (2014), "Three-dimensional centrifuge modelling of pile group responses to side-by-side twin tunnelling", *Tunn. Undergr. Sp. Technol.*, **43**, 350-361. https://doi.org/10.1016/j.tust.2014.05.002.

Oh, D.W., Ahn, H.Y. and Lee, Y.J. (2018), "Behaviour of vertically and horizontally loaded pile and adjacent ground affected by tunnelling", *Geomech. Eng.*, **15**(3), 861-868. https://doi.org/10.12989/gae.2018.15.3.861.

Ong, O.W., Leung, C.F., Yong, K.Y. and Chow, Y.K. (2006), "Pile responses due to tunnelling in clay", *Proceedings of the 6th International Conference on Physical Modelling in Geotechnics Physical Modelling in Geotechnics*, London, U.K., June.

Pang, C.H. (2006), "The effects of tunnel construction on nearby pile foundation", Ph.D. Thesis, The National University of Singapore, Singapore.

Plaxis 3D (2018), *Reference Manual*, in *Plaxis 3D User's Manual*.

Raid R.A.O., Adel A, A.A. and Kadhim A.A. (2016). "Behavior of piled rafts overlying a tunnel in sandy soil", *Geomech. Eng.*, **10**(5), 599-615. https://doi.org/10.12989/gae.2016.10.5.599.

Selemetas, D. (2005), "The response of full-scale piles and piled structures to tunnelling", Ph.D. Thesis, University of Cambridge, U.K.

Selemetas, D., Standing, J.R. and Mair, R.J. (2005), "The response of full-scale piles to tunnelling", *Proceedings of the 5th International Symposium on Geotechnical Aspects of Underground Construction in Soft Ground*, Amsterdam, The Netherlands, June.

Soomro, M.A., Ng, C.W.W., Memon, N.A. and Bhanbhro, R. (2018), "Lateral behaviour of a pile group due to side-by-side twin tunnelling in dry sand: 3D centrifuge tests and numerical modelling", *Comput. Geotech.*, **101**, 48-64. https://doi.org/10.1016/j.compgeo.2018.04.010.

Williamson, M.G. (2014), "Tunnelling effects on bored piles in clay", Ph.D. Thesis, University of Cambridge, Cambridge, U.K.

Xu, Q., Zhu, H., Ma, X., Ma, Z., Li, X., Tang, Z. and Zhuo, K. (2015), "A case history of shield tunnel crossing through group pile foundation of a road bridge with pile underpinning technologies in Shanghai", *Tunn. Undergr. Sp. Technol.*, **45**, 20-33. https://doi.org/10.1016/j.tust.2014.09.002.

You, K.H. and Kim, Y.J. (2017), "A study on numerical modeling method considering gap parameter and backfill grouting of the shield TBM tunnel", *J. Kor. Tunn. Undergr. Sp. Assoc.*, **19**(5), 799-812. https://doi.org/10.9711/KTAJ.2017.19.5.799.

CC